

# UV-Vis-NIR Laser Desorption/Ionization of Synthetic Polymers Assisted by Gold Nanospheres, Nanorods and Nanostars

Francisco Gámez · Paola Hurtado · Paula M. Castillo ·  
Carlos Caro · Ana R. Hortal · Paula Zaderenko ·  
Bruno Martínez-Haya

Received: 16 September 2009 / Accepted: 13 January 2010 / Published online: 28 January 2010  
© Springer Science+Business Media, LLC 2010

**Abstract** The laser desorption/ionization (LDI) assisted by gold nanospheres, nanorods and nanostars has been investigated. Laser fluence thresholds for the appearance of cationized adducts of a polydispersed polyether standard (polyethyleneglycol PEG600) have been determined at the near ultraviolet–visible–near infrared wavelengths delivered by a Nd:YAG laser (266, 355, 532, 1,064 nm). The results demonstrate the efficiency of surface plasmon excitation to assist laser desorption/ionization at laser wavelengths extending to the visible and near infrared, with advantages with respect to conventional LDI techniques using ultraviolet wavelengths. A close correlation is found between the optical absorbance of the nanoparticles and the LDI thresholds, although for the nanospheres plasmonic excitation in the visible appears to be more efficient than non-plasmonic excitation at shorter UV wavelengths. The recorded molecular weight distributions for the PEG600 standard show that the LDI process tends to be less efficient for the heavier components of the polymer mixture, presumably as a consequence of their stronger bonding to the nanoparticle substrate. The role of the coating agent of the nanoparticles in the observed LDI behavior is discussed.

**Keywords** Nanoparticles · Laser desorption · Plasmon excitation · Laser · Mass spectrometry · Molecular sensors · Synthetic polymers

## Introduction

The use of metal nanoparticles as substrates for laser desorption/ionization (LDI) is currently attracting renewed attention. Even though the concept was demonstrated more than two decades ago [1–4], it has been within the last few years that the consolidation of nanoparticle synthesis techniques has catalyzed systematic studies in this field [5–20]. There is a growing interest in the application of plasmonic LDI, in particular, to organic and biochemical analysis and in the development of novel molecular sensors [19–23].

LDI techniques based on nanostructures share the ability to overcome practical limitations of more conventional matrix-assisted LDI employing organic matrices (MALDI). On one hand, they avoid the common problems related to the physicochemical compatibility between matrix and analytes, which in practice makes the choice of the adequate organic MALDI matrix largely a trial-and-error procedure [24]. Moreover, one fundamental advantage of plasmonic nanoparticle substrates with respect to semiconducting materials relies on the tunability of the plasmon excitation, e.g. by controlling the size and geometry of the nanoparticles [25–29]. For LDI applications, this unique feature paves the ground for the use of a single material for broadband laser irradiation. Laser excitation in the visible and longer wavelengths is often advantageous for the detection of labile UV-absorbing species. Furthermore, it allows for the application of a range of alternative laser sources.

Plasmon excitation yields large electromagnetic field and charge interactions in the vicinity of the particle surface. The subsequent energy and charge transfer processes involved in the desorption/ionization

F. Gámez · P. Hurtado · P. M. Castillo · C. Caro ·  
A. R. Hortal · P. Zaderenko · B. Martínez-Haya (✉)  
Departamento de Sistemas Físicos, Químicos y Naturales,  
Universidad Pablo de Olavide, 41013 Seville, Spain  
e-mail: bmarhay@upo.es

mechanisms assisted by the plasmon constitute exciting topics of fundamental research. The present work intends to provide a systematic study of the laser wavelength dependence of the LDI of model synthetic polymers assisted by gold nanoparticles with three different geometries (spheres, rods, stars). The four wavelengths (UV-vis-NIR) delivered by a Nd:YAG laser are employed to probe the broadband LDI behavior of the three materials. Wavelength dependent studies are relatively scarce, as most previous experiments have employed the 337 nm wavelength (nitrogen laser) of the commercial MALDI equipments. Chen and coworkers compared LDI at 355 nm and 532 nm on gold nanorods [9, 10], and LDI at 532 nm and 1064 nm on gold ablated films [15]. They concluded that the plasmonic resonant 532 nm wavelength was most efficient. Spencer and coworkers employed a tunable dye laser to scan the visible plasmonic band of gold nanospheres suspended in aerosols, and found negligible LDI signal in the region of weak absorbance (wavelengths longer than 600 nm) [11]. In contrast, Schürenberg and coworkers reported a weak dependence on laser wavelength in LDI processes assisted by different conducting nanoparticles dispersed in glycerol [4].

We have undertaken an extension of the above-mentioned Au-assisted LDI studies, with the aim to provide further information about the dominant processes involved. “[Experiments](#)” section describes the methods applied for the synthesis and characterization of the nanoparticles, the preparation of the samples, and the equipment employed for the LDI measurements. A detailed account of the results and the main conclusions of our study are provided in “[Results](#)” and “[Summary and conclusions](#)” sections.

## Experiments

### Nanoparticle synthesis and characterization

Gold nanospheres, nanorods and nanostars were synthesized with the procedures outlined below. All chemicals were commercial reagent grade and used as received. Standard polydispersed polyethylene glycol (PEG600) was purchased from Fluka; Hydrogen tetrachloroaurate(III) hydrate from Alfa Aesar; tri-sodium citrate 2-hydrate, silver nitrate and L(+)-ascorbic acid from Panreac; polyvinylpyrrolidone (PVP, average mol. weight  $\sim 10,000$ ), cetyltrimethylammonium bromide, sodium sulfide and *N,N*-dimethylformamide (DMF) from Sigma–Aldrich. Water was purified using a Milli-Q reagent grade water system from Millipore.

Transmission Electron Microscopy (TEM) images of the nanoparticles were taken using a Philips CM200 microscope. The TEM samples were prepared by air drying a drop of an aqueous solution of nanoparticles on a copper grid coated with a carbon film. Illustrative

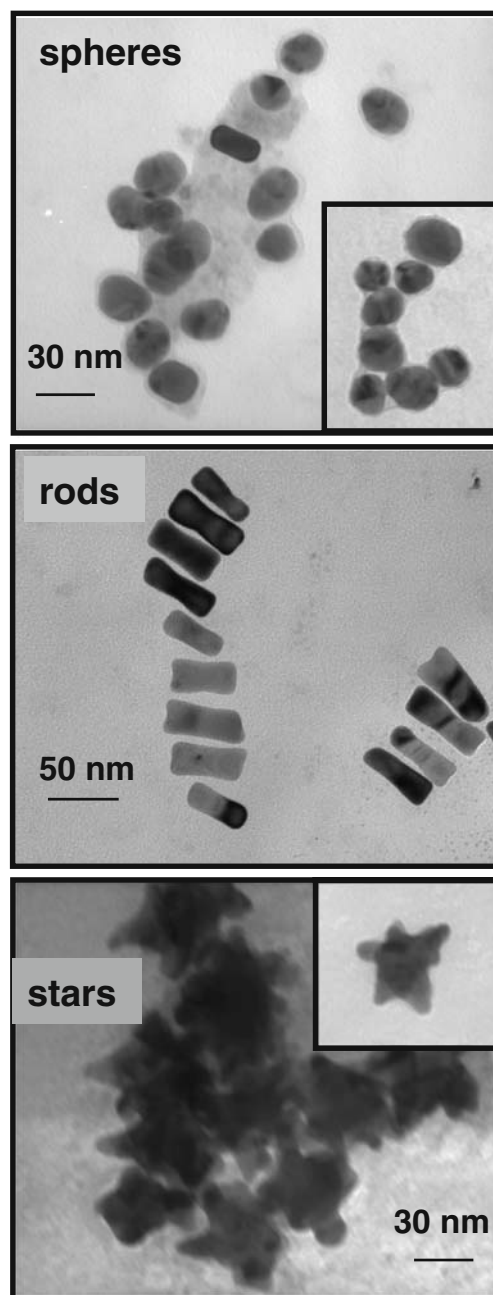


**Fig. 1** Transmission electron microscopy (TEM) images of the three types of gold nanoparticles employed in the present LDI investigation. The nanospheres (*top*) have a 20 nm average diameter and are protected with citrate coating. The nanorods (*middle*) have a length of 50 nm and an average diameter of 18 nm. The nanostars (*bottom*) have average diameters of 35 nm (*core*) and 50 nm (*whole particle*), and are protected with a polyvinylpyrrolidone polymer of average molecular weight  $\sim 10,000$

TEM images are shown in Fig. 1. UV-vis-NIR absorption spectra of the nanoparticles were recorded with an optical fiber CCD spectrometer (DH2000, Ocean optics). The optical absorbances were measured both from an aqueous dispersion and from thin films deposited on quartz. Thin films were produced by precipitation of nanoparticle and nanoparticle/PEG solutions on a quartz plate after evaporation of the solvent in air. Fig. 2 shows that the absorption spectra of the three types of the nanoparticles feature distinct plasmonic bands and cover a broad UV-vis-NIR range.

Spherical citrate-capped gold nanoparticles were synthesized according to a established protocol [30]. Briefly, an aqueous solution of tri-sodium citrate (34 mM, 3 mL) was added, all at once under vigorous

stirring, to an aqueous solution of  $\text{HAuCl}_4$  (0.259 mM, 200 mL) previously heated to 90°C. The reaction mixture was maintained at 90°C under stirring for 10–15 min, until ruby-red color development was complete. The gold nanospheres employed in the present study had an average diameter of 20 nm (Fig. 1, top). The gold nanosphere working solution had an optical density of 0.95 at the 532 nm of the Nd:YAG laser and of 0.85 at 506 nm. Considering the absolute extinction coefficients reported in ref. [31], the concentration of the nanospheres in our working solution is estimated to be  $\approx 1$  nM. This value is consistent with the total reduction of the Au employed in the synthesis.

Gold nanorods were prepared with the procedure described by Sau and Murphy [32]. Aqueous solutions of  $\text{HAuCl}_4$  (10 mM, 250  $\mu\text{L}$ ) and CTAB (100 mM, 7.5 mL) were gently mixed. When the solution turned light brown–yellow in color, an ice-cold aqueous solution of  $\text{NaBH}_4$  (10 mM, 600  $\mu\text{L}$ ) was added and gently mixed for 2 min. The resulting “seed solution” was stored at 25°C. In a second step,  $\text{HAuCl}_4$  (10 mM, 200  $\mu\text{L}$ ),  $\text{AgNO}_3$  (10 mM, 30  $\mu\text{L}$ ), ascorbic acid (100 mM, 32  $\mu\text{L}$ ) and 10  $\mu\text{L}$  of the seed solution were added, in the order indicated, to an aqueous solution of CTAB (100 mM, 4.75 mL). The reaction mixture was gently mixed and left undisturbed for 20 min. Blue color development indicated the formation of the nanorods, which were finally stabilized by addition of sodium sulfide (1.25 mM, 7.35 mL; molar ratio of sulfur to total metal content of 4:1) [33]. The TEM images show that the gold nanorods have a slight dumbbell shape, with average length of 50 nm, maximum diameter of 18 nm and a smaller central diameter of 16 nm (Fig. 1, middle). The gold nanorod working solution had an optical density of 0.20 at 532 nm. We are not aware of absolute extinction coefficients for gold nanorods, but they can be expected to be significantly greater in the visible region than for the nanospheres [25]. Similar considerations hold for the nanostars described below [34]. In agreement with this expectation, the assumption of complete gold reduction in the synthesis leads to concentration of the nanorods in the working solution an estimation of 0.1 nM (i.e., one order of magnitude smaller than the one estimated above for the nanospheres).

Gold nanostars were prepared in a three-step procedure [35], simpler in practice than that of the nanorods. A “seed solution” was prepared by adding an aqueous solution of tri-sodium citrate (3.4 mM, 7.5 mL) to a boiling aqueous solution of  $\text{HAuCl}_4$  (0.42 mM, 30 mL) under vigorous stirring. Boiling was continued for 11 min and stirring for additional 15 min. A “growth solution” was prepared by adding aqueous solution of

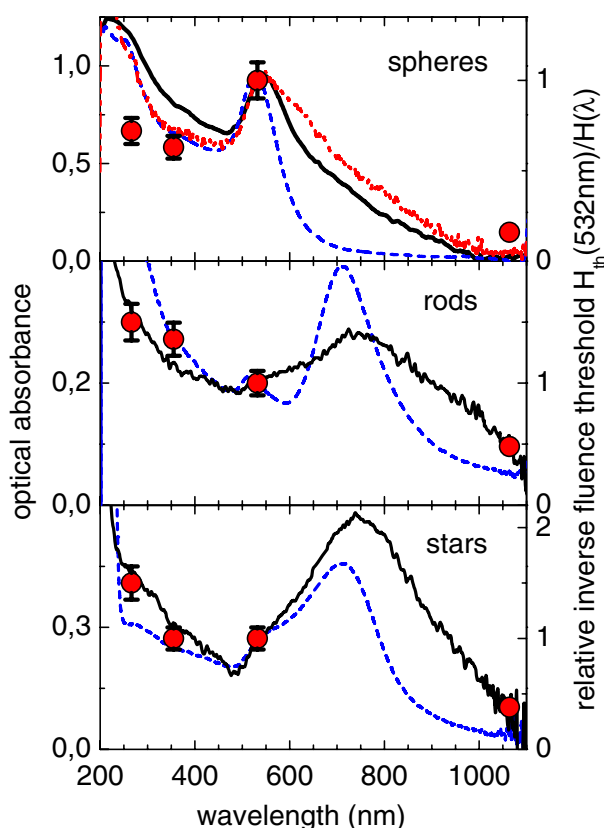


**Fig. 2** Optical absorbance of the gold nanospheres (*top*), nanorods (*middle*) and nanostars (*bottom*) in aqueous solution (*dotted lines*) and in a thin film of each of the nanoparticles deposited on quartz (*solid lines*). The top panel also includes the spectrum measured for a film of nanospheres precipitated with PEG (*dotted dashed curve*). The thin film spectra have been arbitrarily scaled to match the value of the solution spectra at 532 nm (left-hand y-axis). The plasmon bands account for the absorbance above 400 nm, extending to the near-infrared. Relative inverse LDI laser fluence thresholds,  $H_{\text{th}}(532 \text{ nm})/H_{\text{th}}(\lambda)$ , are represented (*circles with error bars*, referred to the right-hand y-axis) to illustrate the degree of correlation between the fluence thresholds and the optical densities at the different wavelengths

HAuCl<sub>4</sub> (50 mM, 84  $\mu$ L) to a solution of PVP in DMF (10 mM, 15 mL) under vigorous stirring at room temperature. Finally, 400  $\mu$ L of seed solution were injected under vigorous stirring to the growth solution and the reaction mixture was stirred for 10–15 min, until blue color development was complete. Nanostars were recovered by centrifugation, washed with Milli-Q water and resuspended in 10 mL Milli-Q water. The size of the gold nanostars achieved for this investigation can be described by an average internal diameter of 35 nm (central core) and an external diameter (including the rod-like protuberances) of 50 nm (Fig. 1, bottom). The gold nanostar working solution had an optical density of 0.27 at 532 nm. An estimated concentration of nanostars of roughly 0.08 nM results from assuming the total reduction of the gold employed in the synthesis.

#### Laser desorption/ionization mass spectrometry

A polydispersed polyethylene glycol standard (PEG600) was chosen for our systematic LDI investigation. The thermochemical stability and appreciable alkali cation affinity of the ether moieties make them particularly suitable for laser desorption/ionization studies [16, 36, 37]. PEG is easily cationized by the ubiquitous Na<sup>+</sup> and K<sup>+</sup> impurities. We added a small amount of Na<sup>+</sup> salt to our samples in order to maintain a constant concentration of cationizing agent in the different substrates. In the present context, PEG cationization is advantageous as it provides a simpler framework in comparison to chemical ionization via proton transfer. Proton sources from the metal nanoparticle substrates are uncertain, unless specific acidic groups or buffers are incorporated to the surface [12, 16]. The LDI PEG–Na<sup>+</sup> ion yields can then be expected to resemble more closely desorption efficiencies, decoupled from complex secondary ionization processes.

Sample solutions for the LDI measurements were prepared by adding 100  $\mu$ L aliquots of a methanol:water (0.1:1) solution 1 mM in PEG600 and 0.1 mM in the cationizing agent (NaI or NaCl), to 100  $\mu$ L of the aqueous dispersions of the gold nanoparticles described above. The LDI samples were then produced with the conventional dried-droplet method: 10  $\mu$ L of sample solution were spotted all at once on the stainless-steel sample plate, covering its *ca.* 20 mm<sup>2</sup> area, and allowed to dry in air. NaI was chosen as cationizing because of its relatively small lattice energy (705 kJ mol<sup>-1</sup>), which ensures a large yield of free Na<sup>+</sup> ions in the desorbing plume to assist PEG cationization. The use of NaCl yielded similar relative LDI thresholds, but the recorded signals were overall weaker due to the

comparably greater lattice energy of the salt (790 kJ mol<sup>-1</sup>) [36]. The use of NaI also served to test the robustness of the substrates against the addition of I<sup>-</sup>. Previous studies have shown that the presence of iodate enhances aggregation of the nanoparticles and deteriorates the LDI signal [38, 39]. In our experiments, such effects were only noticeable when the sample concentration of NaI was increased roughly fivefold with respect to the one employed for the bulk of the present measurements.

LDI mass spectrometry measurements were performed in a reflectron time-of-flight mass spectrometer (RETOF-MS) from Jordan TOF Products Inc. (Grass Valley, CA, USA). The apparatus has been employed in a number of previous LDI investigations of our group (e.g., see ref. [36]) and is described here only briefly. The sample plate is mounted on the repeller plate of the ion source. For the present measurements, the positive analyte ions were accelerated with a total voltage drop of 4.2 kV, applied with a 1  $\mu$ s delay with respect to the laser pulse. The reflectron was operated with a 4.5 kV voltage rise to reflect the ions toward the multichannel-plate detector. Under these operating conditions, the mass resolution of the LDI spectra was  $M/\Delta M \approx 2,000$  for the molecular weights of interest.

The laser radiation employed corresponded to the fundamental and harmonics (1064 nm, 532 nm, 355 nm, 266 nm) of a Nd:YAG laser (Minilite II, Continuum Inc.). All the experiments were performed with the laser beam focused on the sample plate, with lenses of 25 cm (UV-vis) or 20 cm (NIR) nominal focal length, providing focal waists of *ca.* 100  $\mu$ m and 80  $\mu$ m, respectively. The precise focal length for each wavelength was determined by the size and intensity of the focal spot, as measured on a burn paper sheet mounted on a travelling stage. Laser pulses with 5 ns duration and energies ranging 1–100  $\mu$ J were applied. Pulse energies throughout the text refer to values on the sample, i.e., after calibration to account for losses due to optical components and windows. The mass spectra were averaged over 128 laser shots, at 10 shots/s operation.

#### Determination of LDI thresholds

The LDI thresholds were conveniently defined as the laser fluence (energy per unit area),  $H_{th}(\lambda)$ , required to record mass spectra with the major PEG–Na<sup>+</sup> adduct peaks having a signal-to-noise ratio of  $S/N \approx 3$ . The experiments were repeated on up to five independent samples of similar composition, taking different orders for the application of each of the four Nd:YAG wavelengths. Sample-to-sample variation of the *relative* values of the thresholds observed at the four wavelengths

on each sample was within 15 % (range between the lowest and the highest thresholds measured for the set of five samples, relative to the average value). On the other hand, sample-to-sample variations in the *absolute* threshold energies determined in the experiments were within 30 %. This appreciable experimental deviation can be attributed to the heterogeneous precipitation of the sample leading to local "sweet spots" of greater LDI efficiency. In order to minimize this latter sweet-spot effect, the sample plate was continuously rotated during the data collection. Sample preparation with a spin coating methodology did not improve the reproducibility.

### Results

The first step of the investigation was the characterization of the UV-vis-NIR absorption spectra of the nanoparticles, both in solution and in thin films. Such spectra are shown in Fig. 2 where, for direct comparison, the curves for the films have been arbitrarily scaled as to match the absorbance of the aqueous dispersions at 532 nm. On one hand, the nanoparticles display a strong absorbance at short UV wavelengths (< 400 nm) associated to excitations of valence electrons to the conduction band. On the other hand, the plasmon excitation bands cover a broad region of longer wavelengths in the visible and near-infrared. Plasmon absorbance in the gold nanospheres leads to a characteristic band centered in the range 500–600 nm (e.g., see ref. [11]). The broader spectra of the nanorods and the nanostars

are qualitatively similar to each other. Both spectra feature a shoulder located at a similar visible wavelength as the nanosphere plasmon, associated with the excitation of transversal plasmons. In addition, the stronger longitudinal plasmon leads to a prominent absorption band centered around 700–800 nm and extending to the near infrared. The observation of the transversal/longitudinal plasmonic bands is characteristic of the gold nanorods [25, 29]. In the nanostars these bands result from the rod-like shape of the protuberances of the star geometry [29, 34, 40].

Figure 2 also shows that the plasmon bands of the solid films are systematically broadened toward the infrared with respect to those of the corresponding particle solutions. This feature can be attributed to distortion of the plasmonic absorption due to the interaction of the nanoparticles with each other upon evaporation of the solvent [29]. The coprecipitation of the nanospheres with the PEG analyte induces only a slight additional broadening of the spectrum. We did not succeed in measuring similar nanorod/PEG and nanostar/PEG film spectra due to the smaller concentration of the nanoparticles. Nevertheless, broadening effects due to PEG for the nanorods and nanostars can be expected to be of similar or lesser importance than for the nanospheres due to their more bulky coating agents.

The broadband absorbance displayed by the nanoparticles is *a priori* appropriate for LDI applications with UV-vis-NIR laser wavelengths. Table 1 lists the absolute fluence thresholds,  $H_{th}(\lambda)$ , measured in the LDI of PEG600 assisted by each of the nanoparticles

**Table 1** Laser pulse energy ( $E_{th}$ ,  $\mu\text{J}$ ) and fluence ( $H_{th}$ ,  $\text{kJ m}^{-2}$ ) thresholds for the LDI detection of PEG600 with signal/noise ratio  $S/N \approx 3$ , obtained with the gold nanosphere, nanorod and nanostar substrates

Substrate	266 nm	355 nm	532 nm	1,064 nm	
Spheres	$E_{th}(\lambda)$	7	8	5	20
	$H_{th}(\lambda)$	0.89	1.02	0.64	3.96
	$H_{th}(532\text{nm})/H_{th}(\lambda)$	0.72	0.63	1.00	0.16
	$A(\lambda)/A(532\text{nm})$	1.25	0.87	1.00	0.03
Rods	$E_{th}(\lambda)$	20	22	30	40
	$H_{th}(\lambda)$	2.55	2.80	3.82	7.97
	$H_{th}(532\text{nm})/H_{th}(\lambda)$	1.50	1.36	1.00	0.48
	$A(\lambda)/A(532\text{nm})$	1.70	1.60	1.00	0.55
Stars	$E_{th}(\lambda)$	6	9	9	15
	$H_{th}(\lambda)$	0.76	1.14	1.14	2.98
	$H_{th}(532\text{nm})/H_{th}(\lambda)$	1.50	1.00	1.00	0.38
	$A(\lambda)/A(532\text{nm})$	1.60	1.15	1.00	0.32

The relative *inverse* fluence thresholds, normalized with respect to the value at 532 nm,  $H_{th}(532\text{nm})/H_{th}(\lambda)$ , and the relative optical absorbances of the nanoparticle substrates,  $A(\lambda)/A(532\text{nm})$ , are also included in the table. The degree of correlation between these two relative quantities is illustrated in Fig. 2 and serves to evaluate the thermal character of the desorption/ionization mechanism

at the four Nd:YAG laser wavelengths presently considered. As can be observed, under our experimental conditions, fluences within  $0.7\text{--}8.0\text{ kJ m}^{-2}$  (pulse energies within  $6\text{--}40\ \mu\text{J}$ ) were required for threshold detection (signal/noise  $S/N = 3$ ). Figure 2 illustrates the correlation found between the optical absorption of the nanoparticles and the *relative* laser fluence thresholds for the LDI production of the PEG600– $\text{Na}^+$  adducts at the four wavelengths explored. Smaller thresholds are consistently observed at the wavelengths of greater optical absorbance of the nanoparticles. Hence, in order to provide a clearer representation of such correlation, Fig. 2 presents an overlay of the absorption spectra with the *inverse* of each relative threshold fluence, normalized with respect to 532 nm. Furthermore, the axis corresponding to the inverse threshold and absorbance graphs are arbitrarily scaled so that the two magnitudes overlap visually at 532 nm in each case. Such scaling provides an intuitive illustration of the remarkable degree of correlation found between the relative values of inverse thresholds,  $H_{\text{th}}(532\text{ nm})/H_{\text{th}}(\lambda)$ , and the relative absorbances  $A(\lambda)/A(532\text{ nm})$ , at the four wavelengths scoped in our study.

We discuss in the first place the results obtained for the nanospheres. Previous studies with gold nanospheres have primarily employed the 337 nm wavelength of the  $\text{N}_2$  laser, most common in commercial MALDI equipments, hence exciting the nanoparticles outside the plasmon band. Our experiments yield a particularly low threshold ( $0.64\text{ kJ m}^{-2}$ ) at 532 nm, which lies on the maximum of the differentiated plasmonic band. At the two shorter UV wavelengths 266 nm and 355 nm, both inside the valence electron band (i.e., negligible plasmonic excitation), the threshold increases appreciably, by *ca.* 40–60 % (to 0.89 and  $1.02\text{ kJ m}^{-2}$ , respectively). This finding is remarkable, since the absorbance measured for the substrate is for instance significantly greater at 266 nm with respect to 532 nm. Plasmonic excitation seems therefore to be more efficient than valence electron excitation in promoting the LDI process. Finally, at 1064 nm the observation of the PEG polymers required a comparably high threshold fluence of  $\sim 4\text{ kJ m}^{-2}$ . Nevertheless, the substrate produces good quality LDI mass spectra at 1064 nm (see below). The only previous systematic wavelength dependence study of the LDI response of gold nanospheres was performed under quite different experimental conditions [11]. It employed an aerosol suspension of the nanoparticles, and involved laser energies two orders of magnitude higher than the present ones. In the aerosol experiments, no LDI signal was detected at any wavelength for nanospheres with diam-

eters of tens of nanometers. The measurements with 5 nm nanospheres led to a close correlation of the LDI yield with the plasmon absorbance spectrum. The present results corroborate the efficiency of plasmon excitation in promoting LDI reported in the aerosol experiments, extend the range of applicability of the technique to the near infrared, and show that the more conventional LDI conditions presently applied allow for a broader range of nanoparticle sizes than the aerosol approach.

For the gold nanorods and nanostars, a remarkably close correlation is found between the relative laser fluence thresholds and the optical absorbances at the four wavelengths scoped in our study (see Fig. 2). Hence, valence electron excitation in the UV seems to have a similar LDI efficiency as plasmon excitation in the visible and NIR (relative to absorbance). Table 1 shows that  $[A(\lambda)/A(532\text{ nm})] \cdot [H_{\text{th}}(532\text{ nm})/H_{\text{th}}(\lambda)]^{-1} = 1.0 \pm 0.2$ . Hence, the product laser fluence  $\times$  absorbance at the LDI threshold remains roughly constant at the four wavelengths for these two types of nanoparticles. This behavior indicates that, at least under the present working conditions, the LDI mechanism induced by the nanorods and nanostars is likely to be of photothermal character, not crucially dependent on the type of electronic excitation (valence electron or plasmonic) induced on the nanoparticles. The local heating of the nanoparticles and their environment induced by the laser is directly proportional to the energy absorbed in each laser pulse:  $\Delta T = H \cdot (\rho d C_P)^{-1}$ , where  $\Delta T$  is the increase of temperature,  $H$  the energy absorbed per unit area,  $\rho$  and  $C_P$  the density and thermal capacity of the material, and  $d$  the diffusion length of the heat in the time scale of the laser pulse duration [4, 16]. Since the factor  $(\rho d C_P)^{-1}$  remains constant for a given LDI sample, the heating of the substrate is proportional to the energy absorbed. It follows that, at the LDI thresholds relevant to the present study, the heating fulfills  $(\Delta T)_{\text{th}} \propto A(\lambda) \cdot H_{\text{th}}(\lambda)$ , which for nanorods and nanostars is found in our study to be roughly constant at the four wavelengths investigated. This latter result indicates that the threshold is reached when a similar temperature has been reached on the substrate, independently of the wavelength applied.

The thermal behavior of the nanorods and nanostars is likely to be a consequence of the bulky polymers employed for their stabilization. It seems plausible that the protective agents prevent the direct interaction of the PEG with the nanoparticle core. For the nanorods, the interaction of the PEG with the Au surface would in addition be screened by the strong attraction provided by the cationic sites of the CTAB. The

negatively charged ether oxygens of the PEG chains can lead to attachment with multiple CTAB sites, yielding a total binding energy of several eV [36, 41]. This would also be responsible for the higher absolute fluence thresholds found for the rods in comparison to the spheres and stars. The role of the polymeric coatings in the enhancement of the thermal LDI mechanism is supported by the realization that previous investigations with an array of bare isolated nanorods grown on a non-conducting substrate [9, 10] yielded appreciably higher LDI ion yields from plasmon excitation at 532 nm, in comparison to non-plasmonic excitation at 355 nm, in a qualitatively similar manner as found here for the nanospheres. For the nanospheres the thermal mechanism in the present experiments should still be relevant, if not dominant, but it appears that the light citrate coating allows for a partial exposure of the enhanced local field and charge effects associated with plasmon excitation.

Figure 3 displays typical LDI RETOF-MS spectra of the PEG-Na<sup>+</sup> adducts recorded above threshold. The spectra have been selected having ~5 meV signal in the main PEG600-Na<sup>+</sup> adduct peaks. They serve to

illustrate the overall quality of the molecular weight distributions measured at moderate laser energies with the gold nanoparticles presently explored. The three types of nanoparticles yielded well resolved mass distributions of the PEG at the four wavelengths considered, although a different laser fluence had to be employed in each case to achieve similar signal/noise ratios. The number of monomers of the PEG chain corresponding to each of the PEG-Na<sup>+</sup> peaks detected is indicated in the spectra. Background signal from Au<sup>+</sup>, Au<sub>2</sub><sup>+</sup> and Au<sub>3</sub><sup>+</sup> ions desorbed from the substrates and from low mass impurities ( $m/z < 300$ ) is also observed. The use of a polydispersed PEG standard in the present study serves to evaluate the molecular weight selectivity of the LDI process and, hence, its ability to determine reliable molecular weight distributions of synthetic polymers. The most abundant chain length of the PEG600 standard is  $n = 14$  ( $m/z = 657$  for the PEG-Na<sup>+</sup> adduct; *e.g.*, see ref. [42]). In the LDI MS spectra with the three substrates, the most intense peaks in the PEG distribution correspond to  $n = 11$ –12 for the three UV-vis laser wavelengths, and to  $n = 12$ –13 for 1064 nm. Hence, a sizeable shift of the LDI

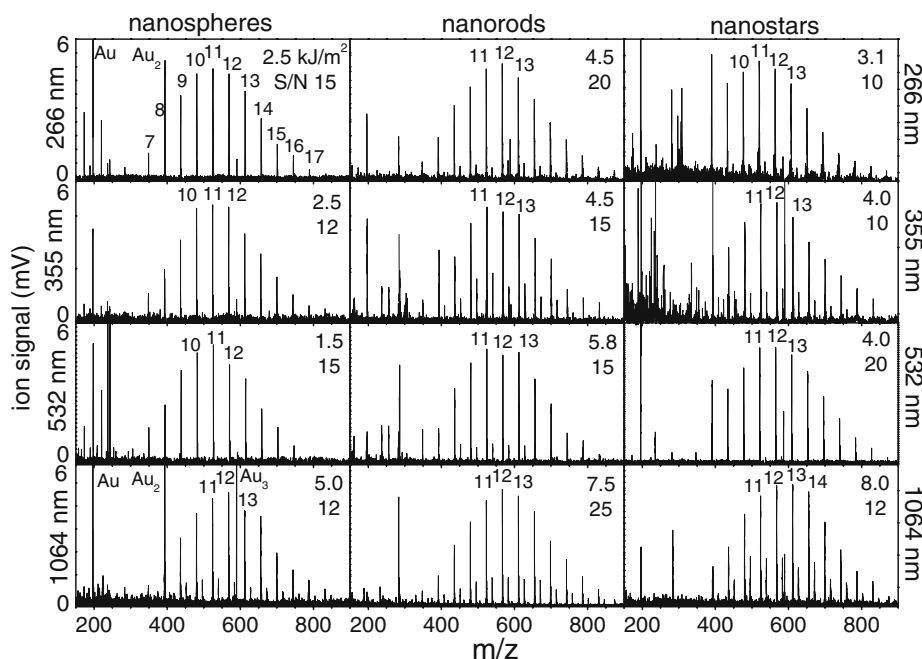


**Fig. 3** Typical LDI RETOF-MS spectra of PEG600 deposited on the gold nanospheres (*left*), nanorods (*center*) and nanostars (*right*), recorded at the four laser wavelengths of the present investigation (266–1,064 nm, *top to bottom*). The spectra have selected as to have ~5 meV signal in the main PEG600-Na<sup>+</sup> adduct peaks. The laser pulse fluence ( $H_{th}$ ) applied and the signal/noise ratio (S/N) achieved in the spectra are indicated in each panel. The main peak distribution around  $m/z = 400$ –800 corresponds

to PEG600-Na<sup>+</sup> adducts. The peaks are labelled according to the number of monomers  $n$  in the HO(CH<sub>2</sub>CH<sub>2</sub>O) <sub>$n$</sub> H polyether chain (for most panels only the most intense peaks are labelled). A weak distribution of PEG600-K<sup>+</sup> from residual potassium present in the sample is occasionally observed. Peaks associated to Au<sup>+</sup>, Au<sub>2</sub><sup>+</sup> and Au<sub>3</sub><sup>+</sup> particles ablated from the nanoparticles are indicated. Several peaks from additives and protective agents are also observed at low masses ( $m/z < 300$ )

peak distribution toward lower masses is observed with respect to the actual molecular weight distribution of the polymers. A similar decrease in detection sensitivity with growing polymer size resulted from previous LDI studies employing nanoparticles of metals other than gold [16]. The reduced LDI signal for the higher masses can be attributed to the stronger attachment of the longer polymeric chains to the nanoparticles. The spectra in Fig. 3 show that for the three nanoparticles, the shift of the distribution is less marked at 1064 nm in comparison to the shorter wavelengths, likely due to the greater laser fluences required to produce the spectra. The high laser fluences applied to the nanorods to initiate the LDI process seems also to compensate for the stronger binding of the PEG polymers to the CTAB coating, leading to molecular weight distributions not too dissimilar from those of the nanostars.

### Summary and conclusions

The performance of gold nanospheres, nanorods and nanostars as substrates to assist the laser desorption/ionization of a model polydispersed synthetic polymer has been tested at four wavelengths covering the UV, visible and near infrared ranges. The present investigation extends previous studies with gold nanospheres and incorporates the randomly oriented CTAB-protected nanorods, and the PVP-protected gold nanostars as novel LDI substrates. The study has demonstrated the ability of the three types of gold nanoparticles to produce well resolved distributions of cationized adducts of a polydispersed polyether standard at the four wavelengths investigated. It can be concluded that gold nanoparticles may be employed as LDI substrates over a broad range of wavelengths, especially the nanorods and nanostars, due to the extension of their plasmonic bands to the near infrared.

For the gold nanorods and nanostars, a close correlation between the laser fluence thresholds and the optical absorbance is found both in the valence electron excitation region and throughout the plasmonic bands. This observation indicates that a similar local heating of the nanoparticle environment is required to reach the LDI threshold. Consequently, a thermal mechanism, weakly dependent on the type of electronic excitation induced by the laser radiation, is likely to dominate the LDI process assisted by the nanorods and nanostars. For the gold nanospheres, a fair correlation between LDI thresholds and absorbances is also found, although in this case plasmonic excitation of the nanoparticles with visible wavelengths leads to a sizeable increase in the efficiency of the LDI process (relative to ab-

sorbance) with respect to excitation in the UV. This trend can be attributed to the exposure of the plasmonic interaction between the PEG analytes and the Au core of the nanospheres, an effect that would be quenched in the nanorods and nanostars due to the coating with bulky protective agents.

The mass spectra recorded in our study show that the nanoparticle assisted LDI process leads to peak distributions for the polydispersed PEG600 standard that are shifted to lower masses with respect to the true molecular weight distribution. Such effect can be expected for analytes capable of attaching to the nanoparticle material through multiple attachment sites, leading to greater binding energies (and hence, reduced LDI sensitivity) with increasing molecular size.

**Acknowledgements** Funding is acknowledged from the Government of Spain through project CTQ2009-10477, from the Andalusian Health Council through project PI-0070/2008, and from the Innovation and Science Council through projects P07-FQM-02600 and P07-FQM-02595.

### References

1. Tanaka K, Waki H, Ido Y, Akita S, Yoshida Y, Yoshida T (1988) Protein and polymer analyses up to  $m/z$  100000 by laser ionization time-of-flight mass spectrometry. *Rapid Commun Mass Spectrom* 2:151–153. doi:10.1002/rcm.1290020802
2. Sunner J, Dratz E, Chen YCh (1995) Graphite-]assisted laser desorption/ionization time-of-flight mass spectrometry of peptides and proteins from liquid solutions. *Anal Chem* 67:4335–4342. doi:10.1021/ac00119a021
3. Owega S, Lai EPC, Bawagan ADO (1998) Surface plasmon resonance-laser desorption/ionization time-of-flight mass spectrometry. *Anal Chem* 70:2360–2365. doi:10.1021/ac971166u
4. Schürenberg M, Dreisewerd K, Hillenkamp F (1999) Laser desorption/ionization mass spectrometry of peptides and proteins with particle suspension matrixes. *Anal Chem* 71:221–229. doi:10.1021/ac980634c
5. McLean JA, Stumpo KA, Russell DH (2005) Size-selected (2–10 nm) gold nanoparticles for matrix assisted laser desorption ionization of peptides. *J Am Chem Soc* 127:5304–5305. doi:10.1021/ja043907w
6. Vanderpuije BNY, Han G, Rotello VM, Vachet RW (2006) Mixed monolayer-protected gold nanoclusters as selective peptide extraction agents for MALDI-MS analysis. *Anal Chem* 78:5491–5496. doi:10.1021/ac0604181
7. Hua L, Chen JR, Ge L, Tan SN (2007) Silver nanoparticles as matrix for laser desorption/ionization of peptides. *J Nanopart Res* 9:1133–1138. doi:10.1007/s11051-007-9244-4
8. Su CL, Tseng WL (2007) Gold nanoparticles as assisted matrix for determining neutral small carbohydrates through laser desorption/ionization time-of-flight mass spectrometry. *Anal Chem* 79:1626–1633. doi:10.1021/ac061747w
9. Chen LC, Yonehama J, Ueda T, Hori H, Hirakoa K (2007) Visible-laser desorption/ionization on gold nanostructures. *J Mass Spectrom* 42:346–353. doi:10.1002/jms.1165



10. Chen LC, Ueda T, Sagisaka M, Hori, H, Hirakoa K (2007) Visible laser desorption/ionization mass spectrometry using gold nanorods. *J Phys Chem C* 111:2409–2415. doi:10.1021/jp065540i
11. Spencer MT, Furutani H, Oldenburg SJ, Darlington TK, Prather KA (2008) Gold nanoparticles as a matrix for visible-wavelength single-particle matrix-assisted laser desorption/ionization mass spectrometry of small biomolecules. *J Phys Chem C* 112:4803–4090. doi:10.1021/jp076688k
12. Castellana ET, Russell DH (2007) Tailoring nanoparticle surface chemistry to enhance laser desorption ionization of peptides and proteins. *Nano Lett* 7:3023–3025. doi:10.1021/nl071469w
13. Kawasaki H, Yonezawa T, Watanabe T, Arakawa R (2007) Platinum nanoflowers for surface-assisted laser desorption/ionization mass spectrometry of biomolecules. *J Chem Phys C* 11:16278–16283. doi:10.1021/jp075159d
14. Kawasaki H, Sugitani T, Watanabe T, Yonezawa T, Moriwaki H, Arakawa R (2008) Layer-by-layer self-assembled multilayer films of gold nanoparticles for surface-assisted laser desorption/ionization mass spectrometry. *Anal Chem* 80:7524–7533. doi:10.1021/ac800789t
15. Chen LC, Mori K, Hori H, Hirakoa K (2009) Au-assisted visible laser MALDI. *Int J Mass Spectrom* 279:41–46. doi:10.1016/j.ijms.2008.10.005
16. Yonezawa T, Kawasaki H, Tarui A, Watanabe T, Arakawa R, Shimada T, Mafune F (2009) Detailed investigation on the possibility of nanoparticles of various metal elements for surface-assisted laser desorption/ionization mass spectrometry. *Anal Sci* 25:339–346. ISSN: 0910-6340
17. Duan J, Linman MJ, Chen ChY, Cheng QJ (2009) CHCA-modified Au nanoparticles for laser desorption ionization mass spectrometric analysis of peptides. *J Am Soc Mass Spectrom* 20:1530–1539. doi:10.1016/j.jasms.2009.04.009
18. Cioffi N, Colaianni L, Pilolli R, Calvano CD, Palmisano F, Zambonin PG (2009) Silver nanofractals: electrochemical synthesis, XPS characterization and application in LDI-MS/Anal. *Bioanal Chem* 394:1375–1383. doi:10.1007/s00216-009-2820-y
19. Huang YF, Chang HT (2006) Nile red-adsorbed gold nanoparticle matrixes for determining aminothiols through surface-assisted laser desorption/ionization mass spectrometry. *Anal Chem* 78:1485–1493. doi:10.1021/ac0517646
20. Shrivastava K, Wu HF (2008) Applications of silver nanoparticles capped with different functional groups as the matrix and affinity probes in surface-assisted laser desorption/ionization time-of-flight and atmospheric pressure matrix-assisted laser desorption/ionization ion trap mass spectrometry for rapid analysis of sulfur drugs and biothiols in human urine. *Rapid Commun Mass Spectrom* 22:2863–2872. doi:10.1002/rcm.3681
21. Daniel MC, Astruc D (2004) Gold nanoparticles: assembly, supramolecular chemistry, quantum-size-related properties, and applications toward biology, catalysis, and nanotechnology. *Chem Rev* 104:293–346. doi:10.1021/cr030698+
22. Anker JN, Hall WP, Lyandres O, Shah NC, Zhao J, van Duyne RP (2008) Biosensing with plasmonic nanosensors. *Nat Mater* 7:442–453. doi:10.1038/nmat2162
23. Guo Z, Ganawi AAA, Liu Q, He L (2006) Nanomaterials in mass spectrometry ionization and prospects for biological application. *Anal Bioanal Chem* 308:584–592. doi:10.1007/s00216-005-0125-3
24. Batoy SMAB, Akhmetova E, Miladinovic S, Smeal J, Wilkins CL (2008) Developments in MALDI mass spectrometry: the quest for the perfect matrix. *Appl Spectrosc Rev* 43:485–550. doi:10.1080/05704920802108198
25. Link S, El-Sayed MA (2000) Shape and size dependence of radiative, non-radiative and photothermal properties of gold nanocrystals. *Int Rev Phys Chem* 19:409–453. doi:10.1080/01442350050034180
26. Link S, El-Sayed MA (2003) Optical properties and ultrafast dynamics of metallic nanocrystals. *Annu Rev Phys Chem* 54:331–366. doi:10.1146/annurev.physchem.54.011002.103759
27. Zhao J, Pinchuk AO, McMahon JM, Li S, Ausman LK, Atkinson AL, Shatz GC (2008) Methods for describing the electromagnetic properties of silver and gold nanoparticles. *Acc Chem Res* 41:1710–1720. doi:10.1021/ar800028j
28. Moores A, Goettmann F (2006) The plasmon band in noble metal nanoparticles: an introduction to theory and applications. *New J Chem* 30:1121–1132. doi:10.1039/b604038c
29. Pelton M, Aizpurua J, Bryant G (2008) Metal-nanoparticle plasmonics. *Laser & Photon Rev* 2:136–159. doi:10.1002/lpor.200810003
30. Hayat M (1989) *Colloidal gold: principles, methods and applications*. Academic, San Diego
31. Liu X, Atwater M, Wang J, Huo Q (2007) Extinction coefficient of gold nanoparticles with different sizes and different capping ligands. *Colloids Surf B Biointerfaces* 58:3–7. doi:10.1016/j.colsurfb.2006.08.005
32. Sau TK, Murphy CJ (2004) Seeded high yield synthesis of short Au nanorods in aqueous solution. *Langmuir* 20:6414–6420. doi:10.1021/la049463z
33. Zweifel DA, Wei A (2005) Sulfide-arrested growth of gold nanorods. *Chem Mater* 17:4259–4261. doi:10.1021/cm0506858
34. Hao F, Nehl CL, Hafner JH, Nordlander P (2007) Plasmon resonances of a gold nanostar. *Nano Lett* 7:729–732. doi:10.1021/nl062969c
35. Khouri CG, Vo-Dinh T (2008) Gold nanostars for surface-enhanced raman scattering: synthesis, characterization and optimization. *J Phys Chem C* 112:18849–18859. doi:10.1021/jp8054747
36. Hortal AR, Hurtado P, Martínez-Haya B, Arregui A, Bañares L (2008) Solvent-free MALDI investigation of the cationization of linear polyethers with alkali metals. *J Phys Chem B* 112:8530–8535. doi:10.1021/jp802089r
37. Montaudo G, Samperi F, Montaudo MS (2006) Characterization of synthetic polymers by MALDI-MS. *Prog Polym Sci* 31:277–357. doi:10.1016/j.progpolymsci.2005.12.001
38. Cheng WL, Dong SJ, Wang EK (2003) Iodine-induced gold-nanoparticle fusion/fragmentation/aggregation and iodine-linked nanostructured assemblies on a glass substrate. *Angew Chem Int Ed* 42:449–452. doi:10.1002/anie.200390136
39. Stumpo KA, Russell DH (2009) Anion effects on ionization efficiency using gold nanoparticles as matrices for LDI-MS. *J Phys Chem C* 113:1641–1647. doi:10.1021/jp804032z
40. Nehl CL, Liao H, Hafner JH (2006) Optical properties of star-shaped gold nanoparticles. *Nano Lett* 6:683–688. doi:10.1021/nl052409y
41. Armentrout PB (1999) Cation-ether complexes in the gas phase: thermodynamic insight into molecular recognition. *Int J Mass Spectrom* 193:227–240. doi:10.1016/S1387-3806(99)00165-7
42. Robinson EW, Garcia DE, Leib RD, Williams ER (2006) Enhanced mixture analysis of poly(ethylene glycol) using high-field asymmetric waveform ion mobility spectrometry combined with fourier transform ion cyclotron resonance mass spectrometry. *Anal Chem* 78:2190–2198. doi:10.1021/ac051709x